# Response of Freshwater Flux and Sea Surface Salinity to Variability of the Atlantic Warm Pool

CHUNZAI WANG

*NOAA/Atlantic Oceanographic and Meteorological Laboratory, Miami, Florida*

LIPING ZHANG

*Cooperative Institute for Marine and Atmospheric Studies, University of Miami, and NOAA/Atlantic Oceanographic and Meteorological Laboratory, Miami, Florida, and Physical Oceanography Laboratory, Ocean University of China, Qingdao, China*

SANG-KI LEE

*Cooperative Institute for Marine and Atmospheric Studies, University of Miami, and NOAA/Atlantic Oceanographic and Meteorological Laboratory, Miami, Florida*

(Manuscript received 16 May 2012, in final form 10 August 2012)

ABSTRACT

The response of freshwater flux and sea surface salinity (SSS) to the Atlantic warm pool (AWP) variations from seasonal to multidecadal time scales is investigated by using various reanalysis products and observations. All of the datasets show a consistent response for all time scales: A large (small) AWP is associated with a local freshwater gain (loss) to the ocean, less (more) moisture transport across Central America, and a local low (high) SSS. The moisture budget analysis demonstrates that the freshwater change is dominated by the atmospheric mean circulation dynamics, while the effect of thermodynamics is of secondary importance. Further decomposition points out that the contribution of the mean circulation dynamics primarily arises from its divergent part, which mainly reflects the wind divergent change in the low level as a result of SST change. In association with a large (small) AWP, warmer (colder) than normal SST over the tropical North Atlantic can induce anomalous low-level convergence (divergence), which favors anomalous ascent (decent) and thus generates more (less) precipitation. On the other hand, a large (small) AWP weakens (strengthens) the trade wind and its associated westward moisture transport to the eastern North Pacific across Central America, which also favors more (less) moisture residing in the Atlantic and hence more (less) precipitation. The results imply that variability of freshwater flux and ocean salinity in the North Atlantic associated with the AWP may have the potential to affect the Atlantic meridional overturning circulation.

## 1. Introduction

The Atlantic warm pool (AWP), defined by the sea surface temperature (SST) warmer than 28.5°C (Wang and Enfield 2001), comprises the Intra-America Seas (IAS) (i.e., the Gulf of Mexico and the Caribbean) and the western tropical North Atlantic (TNA). Unlike the Indo-Pacific warm pool, which straddles the equator, the AWP is entirely north of the equator and is sandwiched between North and South America and between the tropical North Pacific and Atlantic Ocean. The AWP has a large seasonal cycle. In addition to the seasonal cycle, the AWP shows variability on both interannual and multidecadal time scales as well as a long-term warming trend (Wang et al. 2008a), with large AWPs being almost three times larger than small ones (Wang and Enfield 2003).

Wang et al. (2006) demonstrated that summer rainfall in the Caribbean, Mexico, and the eastern subtropical Atlantic is largely associated with the AWP variability by using a blend of satellite estimates and rain gauge data. Based on the National Center for Atmospheric Research atmospheric model, Wang et al. (2007, 2008b) further

*Corresponding author address:* Dr. Chunzai Wang, NOAA/Atlantic Oceanographic and Meteorological Laboratory, 4301 Rickenbacker Causeway, Miami, FL 33149.
E-mail: chunzai.wang@noaa.gov

DOI: 10.1175/JCLI-D-12-00284.1

showed that the variability of the AWP not only modulates local precipitation but also affects moisture export across Central America to the eastern North Pacific. A large (small) AWP can induce an anomalous ascent (decent) flow and thus leads to a significant response of an increased (decreased) rainfall in the AWP region. Meanwhile, a large (small) AWP weakens (strengthens) the summertime Caribbean low-level jet (CLLJ) (Wang 2007; Wang and Lee 2007) and the associated westward moisture transport, which is also in favor of generating an increased (a decreased) precipitation in the TNA.

However, how evaporation, precipitation, moisture transport and salinity vary with the AWP is poorly known and understood, particularly in long-term observations. The freshwater variation can lead to a salinification or freshening of the subtropical North Atlantic Ocean, which is subsequently carried by the wind-driven ocean circulation (Thorpe et al. 2001; Vellinga and Wu 2004; Yin et al. 2006; Krebs and Timmermann 2007) to high latitudes where water cools and sinks. In this way, net freshwater flux and its corresponding salinity change over the AWP may have the potential to affect deep-water formation and the Atlantic meridional overturning circulation (Zaucker and Broecker 1992; Broecker 1997; Romanova et al. 2004). The purpose of the present paper is to present a quantitative evaluation of the net freshwater flux changes in response to the AWP variation. Since the local salinity response is not only determined by precipitation but also by evaporation, we thus assess the net freshwater flux of evaporation minus precipitation (EmP) associated with the AWP variability. Using several reanalysis products and observations, we examine the physical mechanisms of the net freshwater change associated with the AWP variation on various time scales. Additionally, we also give a quantitative evaluation of the moisture transport across Central America from the Atlantic to the Pacific associated with the AWP variability.

The paper is organized as follows. In the following section, we describe the datasets and methods that are used in this study. Section 3 shows the seasonal cycle of the freshwater flux, associated physical mechanisms, moisture transport, and sea surface salinity (SSS) in the AWP region. Sections 4 and 5 document these variations on interannual and multidecadal time scales. Finally, section 6 gives a summary and discussion.

## 2. Datasets and methodology

### *a. Datasets*

Several atmospheric reanalysis datasets are used in this study. The first one is the National Centers for Environmental Prediction (NCEP)–National Center for Atmospheric Research (NCAR) reanalysis field on a 2.5° × 2.5° latitude–longitude horizontal grid (Kalnay et al. 1996). The data consist of daily fields from 1948 to 2010. The second dataset is from the 40-yr European Centre for Medium-Range Weather Forecasts Re-Analysis (ERA-40) (Gibson et al. 1997), which spans from 1958 to 2001 and also has a horizontal resolution of 2.5° × 2.5°. Another dataset is the Twentieth Century Reanalysis version 2 (20CRv2), which contains the estimate of global tropospheric variability spanning from 1871 to 2010 at a 6-hourly interval and with a spatial resolution of 2° × 2° (Compo et al. 2011). In addition, the global objectively analyzed air–sea fluxes (OAFlux) product (Yu and Weller 2007) is also used to examine the evaporation change associated with the AWP. We also use the Global Precipitation Climatology Project (GPCP) (Adler et al. 2003) that is similar to the Climate Prediction Center (CPC) Merged Analysis of Precipitation (CMAP) (Xie and Arkin 1997). The GPCP dataset blends satellite estimates and rain gauge data on a 2.5° × 2.5° grid from January 1979 to 2010.

Three ocean reanalysis products are also used in this study: the Simple Ocean Data Assimilation (SODA) (Carton and Giese 2008), the German Estimating the Circulation and Climate of the Ocean (GECCO) (Kõhl et al. 2006), and the Geophysical Fluid Dynamics Laboratory (GFDL) (Rosati et al. 2004). The SODA uses an ocean general circulation model to assimilate available temperature and salinity observations. The product is a gridded dataset of oceanic variables with monthly values and a 0.5° × 0.5° horizontal resolution and 40 vertical levels. The version 2.2.4 of the SODA is used, with the time covering from 1871 to 2008. The GECCO is also a monthly product from 1952 to 2001, with a 1° × 1° horizontal resolution and 23 vertical levels. The GFDL ocean reanalysis product is from 1960 to 2004, with a 1° × 1° resolution (enhanced to 1/3° × 1/3° in the tropics between 30°S and 30°N) and 50 vertical levels. Additionally, the objectively analyzed temperature and salinity version 6.7 (Ishii et al. 2006) at 24 levels in the upper ocean of 1500 m from 1945 to 2010 is also used to study the salinity variability associated with the AWP variation. The analysis is based on the World Ocean Database/*World Ocean Atlas 2005* (*WOA05*), the global temperature–salinity in the tropical Pacific from Institut de Recherche pour le Développement (IRD)/France, and the Centennial in situ Observation Based Estimates (COBE) sea surface temperature. The Ishii et al. analysis also includes the Argo profiling buoy data in the final several years and the XBT depth bias correction. Finally, we use the global gridded Argo data from Katsumata and Yoshinari (2010), which has a 1° × 1° horizontal resolution and spans from 2001 to 2010.

### b. Moisture budget

Following Peixoto and Oort (1992) and Trenberth and Guillemot (1995), we can write the vertically integrated moisture equation as

$$(E-P)=\frac{\partial W}{\partial t}+\nabla\cdot\left[g^{-1}\int_0^{p_s}(\mathbf{U}q)\,dp\right], \tag{1}$$

where $W=(1/g)\int_0^{p_s} q\,dp$ is the column-integrated water vapor of the atmosphere; $q$, $\mathbf{U}$, $p_s$, $E$, and $P$ are specific humidity, horizontal velocity, surface pressure, evaporation, and precipitation, respectively. In this paper, $E-P$ is represented by EmP. The second integral on the rhs of Eq. (1) describes the divergence of water vapor horizontal flux. Integrating Eq. (1) over the globe, the divergence term becomes zero. Apparently, any variation in the global-mean water vapor results from an imbalance between global-mean evaporation and precipitation. When time averages of Eq. (1) are taken for a month, the divergence of water vapor flux can be divided into the mean and transient eddy components in the form of

$$\begin{aligned}(\overline{E}-\overline{P})&=\frac{\partial\overline{W}}{\partial t}+\nabla\cdot\left[g^{-1}\int_0^{p_s}(\overline{\mathbf{U}}\overline{q})\,dp\right]\\&\quad+\nabla\cdot\left(g^{-1}\int_0^{p_s}(\overline{\mathbf{U}'q'})\,dp\right)\\&\equiv\frac{\partial\overline{W}}{\partial t}+\mathrm{div}Q_M+\mathrm{div}Q_E.\end{aligned} \tag{2}$$

The overbar indicates monthly mean and the prime represents departure from the monthly mean (by transient eddies). Here $\mathrm{div}Q_M$ represents the moisture flux divergence contributed from the mean (monthly to longer time scales) and $\mathrm{div}Q_E$ is the contribution from transient eddies (submonthly time scales). The water vapor flux divergence can be further broken into the contributions that depend mostly on the mass divergence in the lower atmosphere and horizontal advection by the wind. Thus, Eq. (2) can be decomposed into

$$\begin{aligned}(\overline{E}-\overline{P})&\approx\frac{\partial\overline{W}}{\partial t}+\frac{1}{g}\int_0^{p_s}(\overline{q}\nabla\cdot\overline{\mathbf{U}})\,dp\\&\quad+\frac{1}{g}\int_0^{p_s}(\overline{\mathbf{U}}\cdot\nabla\overline{q})\,dp+\frac{1}{g}\int_0^{p_s}\nabla\cdot(\overline{\mathbf{U}'q'})\,dp.\end{aligned} \tag{3}$$

Note that in Eq. (3) we have neglected the term of $(q_s\mathbf{U}_s\cdot\nabla p_s)/g$ since this term (involved surface quantities) is very small based on our calculation (also see Seager et al. 2010).

We further examine the monthly change by denoting

$$\delta(\cdot)=(\cdot)-(\cdot)_C, \tag{4}$$

where $(\cdot)$ indicates each term of Eq. (3) at every month and $(\cdot)_C$ indicates the long-term annual-mean value. Then, Eq. (3) can be approximated as

$$\begin{aligned}\delta(\overline{E}-\overline{P})&\approx\delta\left(\frac{\partial\overline{W}}{\partial t}\right)+\frac{1}{g}\int_0^{p_s}\delta(\overline{q}\nabla\cdot\overline{\mathbf{U}})\,dp+\frac{1}{g}\int_0^{p_s}\delta(\overline{\mathbf{U}}\cdot\nabla\overline{q})\,dp+\frac{1}{g}\int_0^{p_s}\nabla\cdot\delta(\overline{\mathbf{U}'q'})\,dp\\&=\delta\left(\frac{\partial\overline{W}}{\partial t}\right)+\frac{1}{g}\int_0^{p_s}(\delta\overline{q}\nabla\cdot\overline{\mathbf{U}}_C+\overline{q}_C\nabla\cdot\delta\overline{\mathbf{U}}+\delta\overline{\mathbf{U}}\cdot\nabla\overline{q}_C+\overline{\mathbf{U}}_C\cdot\nabla\delta\overline{q})\,dp+\frac{1}{g}\int_0^{p_s}\nabla\cdot\delta(\overline{\mathbf{U}'q'})\,dp.\end{aligned} \tag{5}$$

Following Seager et al. (2010), terms in Eq. (5) involving change in $q$ but no change in $\mathbf{U}$ (i.e., $\mathbf{U}_C$) are referred to as thermodynamic contributors to the change in column-integrated water vapor, and terms involving change in $\mathbf{U}$ but no change in $q$ (i.e., $q_C$) are referred to as dynamic contributors. Note that the nonlinear term $[\int_o^{p_s}\nabla\cdot(\delta\overline{q}\delta\overline{\mathbf{U}})\,dp]$ that is the product of changes in both time-mean specific humidity and flow is neglected because of its small magnitude. Briefly, the thermodynamic contributions are in the form of

$$\delta\mathrm{TH}=\frac{1}{g}\int_0^{p_s}(\delta\overline{q}\nabla\cdot\overline{\mathbf{U}}_C+\overline{\mathbf{U}}_C\cdot\nabla\delta\overline{q})\,dp\equiv\delta\mathrm{TH}_D+\delta\mathrm{TH}_A \tag{6}$$

and the dynamic contributions are

$$\begin{aligned}\delta\mathrm{MCD}&=\frac{1}{g}\int_0^{p_s}(\overline{q}_C\nabla\cdot\delta\overline{\mathbf{U}}+\delta\overline{\mathbf{U}}\cdot\nabla\overline{q}_C)\,dp\\&\equiv\delta\mathrm{MCD}_D+\delta\mathrm{MCD}_A.\end{aligned} \tag{7}$$

In Eqs. (6) and (7), we can further decompose the thermodynamic and dynamic contributions into terms due to the flow divergence (subscript $D$) and the advection of moisture (subscript $A$),

$$\delta\mathrm{TH}_D=\frac{1}{g}\int_0^{p_s}(\delta\overline{q}\nabla\cdot\overline{\mathbf{U}}_C)\,dp, \tag{8}$$

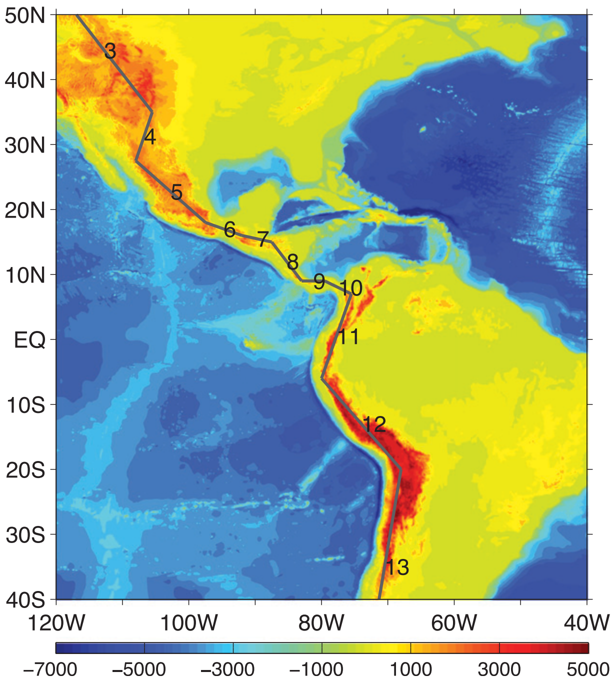


FIG. 1. The 5′ gridded elevations/bathymetry for the world (ETOPO5) orography (m, shading) and the line segments across which moisture transport is calculated (black line). ETOPO5 was generated from a digital database of land and seafloor elevations on a 5′ latitude/longitude grid (which can be downloaded from http://www.usgodae.org/pub/outgoing/static/ocn/bathy/).

$$\delta \mathrm{TH}_A = \frac{1}{g}\int_0^{p_s} (\overline{\mathbf{U}}_C \cdot \nabla \delta \overline{q})\, dp\,, \tag{9}$$

$$\delta \mathrm{MCD}_D = \frac{1}{g}\int_0^{p_s} (\overline{q}_C \nabla \cdot \delta \overline{\mathbf{U}})\, dp\,, \tag{10}$$

$$\delta \mathrm{MCD}_A = \frac{1}{g}\int_0^{p_s} (\delta \overline{\mathbf{U}} \cdot \nabla \overline{q}_C)\, dp\,. \tag{11}$$

All terms in these equations are obtained with the originally daily or monthly data and then are averaged to climatological seasonal cycle and summer (fall) mean time series to focus on various time-scale variations.

### c. Moisture transport

Freshwater flux change over the AWP is influenced by or related to the moisture transport across the Americas from the Atlantic to the Pacific. To calculate moisture transport across the Americas, we use a method suggested by Richter and Xie (2010), who define 13 line segments (Fig. 1) that run approximately along the Atlantic drainage, integrate the moisture flux across each line segment, and thus obtain the cross-isthmus moisture transport. The equation for an individual line segment is

$$\overline{\mathrm{MT}} = \int_p \int_l (\overline{uq})\, dl \frac{dp}{g} = \int_p \int_l (\overline{u}\,\overline{q})\, dl \frac{dp}{g} + \int_p \int_l (\overline{u'q'})\, dl \frac{dp}{g} \equiv \mathrm{MT}_M + \mathrm{MT}_E\,, \tag{12}$$

where MT is the moisture transport across the line segment, $p$ is pressure, $l$ is position along the segment, $q$ is specific humidity, and $g$ is gravity. Here $u$ is the velocity perpendicular to line segments. The overbar indicates monthly mean and the prime indicates departure from the monthly mean. Thus, moisture transport can be decomposed into contributions by the mean ($\mathrm{MT}_M$) and transient eddies ($\mathrm{MT}_E$). Here, we choose the integration from segments 6 to 10 (see Fig. 1): that is, the moisture transport across Central America. A positive value of MT is indicative of a moisture export from the Atlantic to the Pacific basin and vice versa.

## 3. Annual variability

In this section, we first describe the EmP seasonal cycle in the AWP region. We then show physical processes that control the EmP seasonal cycle. The seasonality of the moisture transport across Central America and its relationship with the CLLJ are discussed in next subsection. Finally, we examine the seasonal variability of sea surface salinity (SSS).

### a. EmP seasonal cycle

To show the seasonal cycle of net freshwater flux over the AWP region, we calculate the EmP variation (monthly climatology minus long-term mean) from January to December in the region of 5°–30°N from the American coast to 40°W based on various datasets (Fig. 2, left). Note that evaporation in 20CRv2 and NCEP is computed from the model output of latent heat flux because of the lack of direct evaporation data. As shown in these panels, EmP is characterized by a significant annual cycle, with an excess of freshwater during May–November and a deficit of freshwater in the winter and early spring. The EmP seasonal cycle covaries well with the variation of the AWP (Wang and Enfield 2003), in which the appearance (disappearance) of the AWP from May to November (December to April) (Fig. 2g) coincides with the excess (deficit) of precipitation. As shown in Fig. 2g, the AWP almost does not exist in the winter and spring if the AWP is defined as area of SST greater than 28.5°C. This implies that the AWP plays an important role in modulating local freshwater flux. A further analysis finds that the precipitation change dominates the EmP seasonal cycle, whereas evaporation is of secondary importance (not shown).

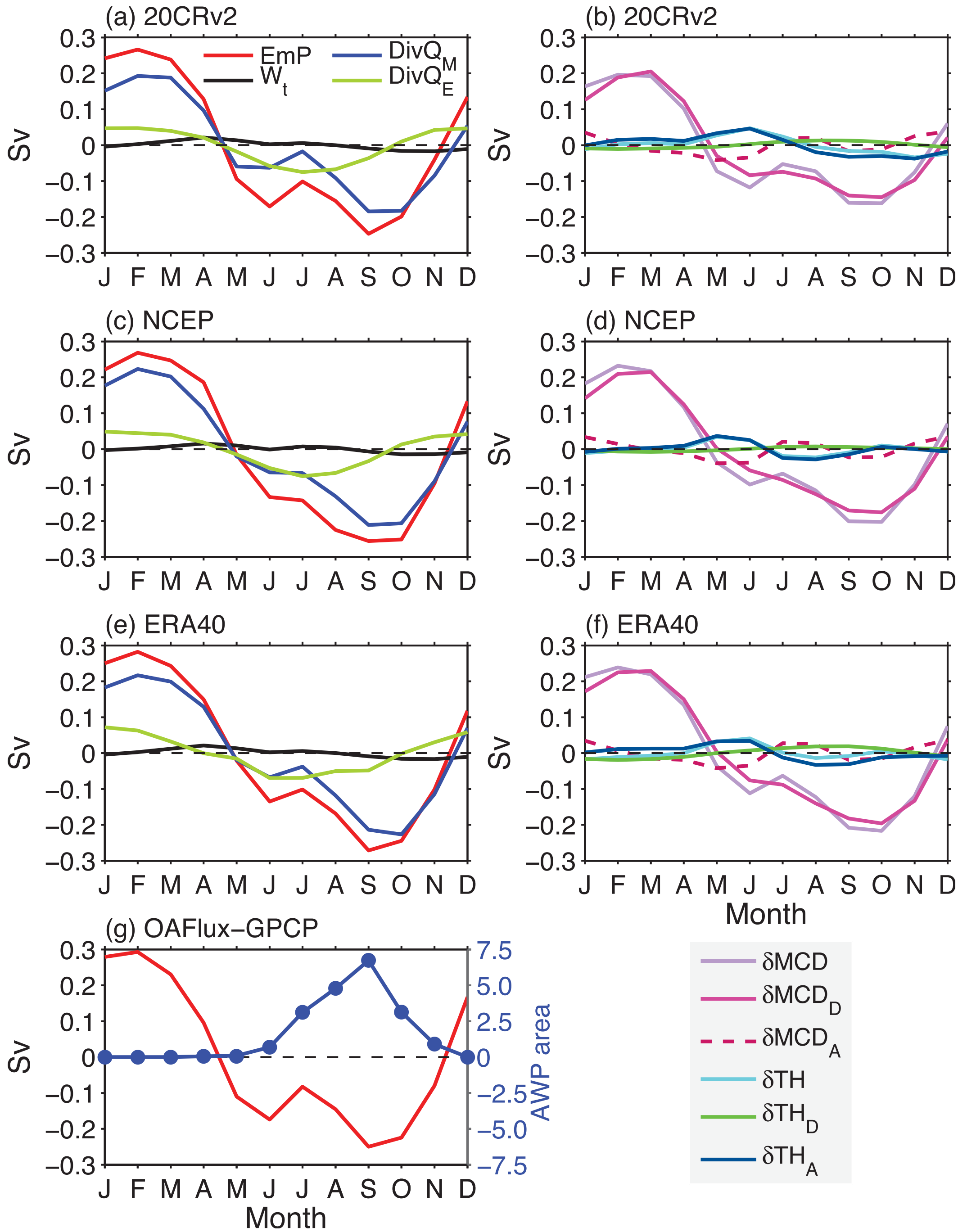


FIG. 2. (left) EmP seasonal cycle and (right) associated moisture budget using the (a),(b) 20CRv2; (c),(d) NCEP; (e),(f) ERA-40; and (g) OAFlux–GPCP datasets. Terms EmP, $W_t$, div$Q_M$, and div$Q_E$ denote the EmP, moisture tendency, and moisture flux divergence contribution from monthly to longer time scales and moisture flux divergence contribution from the transient eddies (submonthly time scale), respectively. The AWP area ($10^{12}$ m$^2$) of SST greater than 28.5°C is also shown in (g). In (b),(d),(f) the contributions from the mean circulation dynamics ($\delta$MCD) and thermodynamics ($\delta$TH) and their corresponding advective parts ($\delta$MCD$_A$ and $\delta$TH$_A$) and convergent parts ($\delta$MCD$_D$ and $\delta$TH$_D$) are represented: units in Sverdrups. The AWP region is in the region of 5°–30°N from the America coast to 40°W.

In general, the EmP annual cycle agrees well among four different datasets of 20CRv2, NCEP, ERA-40, and OAFlux–GPCP. However, some discrepancies still exist. Net freshwater flux calculated from the OAFlux–GPCP precipitation displays an EmP ridge in July, which in turn leads to a weak semiannual feature of EmP. 20CRv2 is a reanalysis dataset that can best reproduce this phenomenon. The EmP ridge in July is predominated by the precipitation (not shown), which is closely related to the well-known phenomenon of the midsummer drought that is more obvious in the regions of Central America and South Mexico (e.g., Magana et al. 1999; Mapes et al. 2005).

### *b. Processes controlling EmP seasonal cycle*

Next, we address how the EmP seasonal cycle is formed or what physical processes controlling the EmP seasonal cycle are. The left panels of Fig. 2 show EmP, the moisture tendency ($\partial\overline{W}/\partial t$), and the moisture flux divergence contributed from the monthly mean (div$Q_M$) and from the transient eddies (div$Q_E$). It is seen that the EmP seasonal cycle in the AWP region can be largely accounted for by div$Q_M$, including moistening in the summer and fall and drying in the winter and spring, while the contribution from moisture tendency is negligible. Given the smallness of moisture tendency, this term is ignored in later discussions. In addition, we find that div$Q_E$ also presents an annual cycle, which is almost in phase with EmP. The contribution from the transient eddies is significant in the summer [June–August (JJA)], but with a smaller magnitude than the mean term of div$Q_M$ in all other seasons. This is not surprising since the AWP resides over the tropics where atmospheric response to the ocean is primarily linear and baroclinic and the transient eddy is not very active.

As derived in section 2, the change of div$Q_M$ can be further separated into the thermodynamics contribution ($\delta$TH) and the contribution from the mean circulation dynamics ($\delta$MCD). The right panels of Fig. 2 show that a large portion of the EmP change can be explained by the mean circulation dynamics of $\delta$MCD, whereas the thermodynamics contribution of $\delta$TH is much smaller. The $\delta$TH can be further decomposed into the effect of the change in humidity gradient when the advective wind is fixed at the climatological mean ($\delta\mathrm{TH}_A$) and the effect of the change in humidity with a fixed climatological divergent wind ($\delta\mathrm{TH}_D$) [see Eqs. (8) and (9)]. It can be found that $\delta$TH is primarily determined by $\delta\mathrm{TH}_A$, while the contribution from $\delta\mathrm{TH}_D$ is negligible. Figure 2 shows that $\delta\mathrm{TH}_A$ is characterized by a net freshwater loss from the ocean in January–July and vice versa in August–December.

The mean circulation dynamics of $\delta$MCD is dominated by $\delta\mathrm{MCD}_D$ which represents the effect of change in the wind divergence with a fixed humidity as can be seen in Eq. (10). Clearly, the positive value of EmP in the winter and early spring (when the AWP disappears) is balanced by an increase in low-level wind divergence, which disfavors precipitation and corresponds to a weakening of the ascent over the AWP region. The opposite is true during the summer and fall when the AWP appears. These results are consistent with previous modeling studies (e.g., Wang et al. 2008b) in which atmospheric response to a large (small) AWP is featured by an anomalous convergence (divergence) in the low level and an upward (a downward) vertical velocity—a classic Gill's pattern response to the tropical heating (Gill 1980).

The other component of $\delta\mathrm{MCD}_A$ is of secondary importance to the EmP change. Differing from other terms, $\delta\mathrm{MCD}_A$ shows a semiannual feature, with a drying effect during the winter and summer and a moistening effect during the other seasons. This is also the determining factor to cause a weak semiannual variability of EmP in 20CRv2 dataset shown in Fig. 2a. In NCEP and ERA-40, the contribution from $\delta\mathrm{MCD}_D$ is too strong to recognize the role of $\delta\mathrm{MCD}_A$, so that a semiannual variability of EmP does not seem to clearly show. It is expected that $\delta\mathrm{MCD}_A$ is largely associated with the wind change since the humidity gradient is fixed as shown in Eq. (11). Over the AWP region, the maximum of easterly zonal wind at 925 hPa occurs in the Caribbean region, which is called the Caribbean low-level jet. As shown by Wang (2007), the CLLJ varies semiannually, with two maxima in the summer and winter and two minima in the fall and spring. It is interesting to find that the semiannual feature in $\delta\mathrm{MCD}_A$ is consistent with the variation of the CLLJ. This suggests that the CLLJ and the associated moisture transport may be closely related to the EmP variation, which will be examined in the following section. Wang (2007) further pointed out that the strength of the CLLJ is closely linked with the meridional SST gradient that is largely fluctuated with the AWP. Therefore, from the dynamical point of view, the AWP can not only induce an anomalous wind divergence to modulate EmP but also modulate EmP by changing SST gradient to induce moisture advection by anomalous wind. Additionally, from the thermodynamical point of view, the AWP can modulate local EmP by changing humidity advection by the anomalous humidity gradient and by changing the water vapor content to affect the moisture divergence.

In summary, the EmP seasonal cycle associated with the AWP is dominated by the AWP-modulated mean circulation dynamics ($\delta$MCD), whereas the thermodynamics contribution ($\delta$TH) plays a much smaller role. Furthermore, the large contribution of the mean circulation dynamics is primarily due to the wind divergence change ($\delta\mathrm{MCD}_D$).

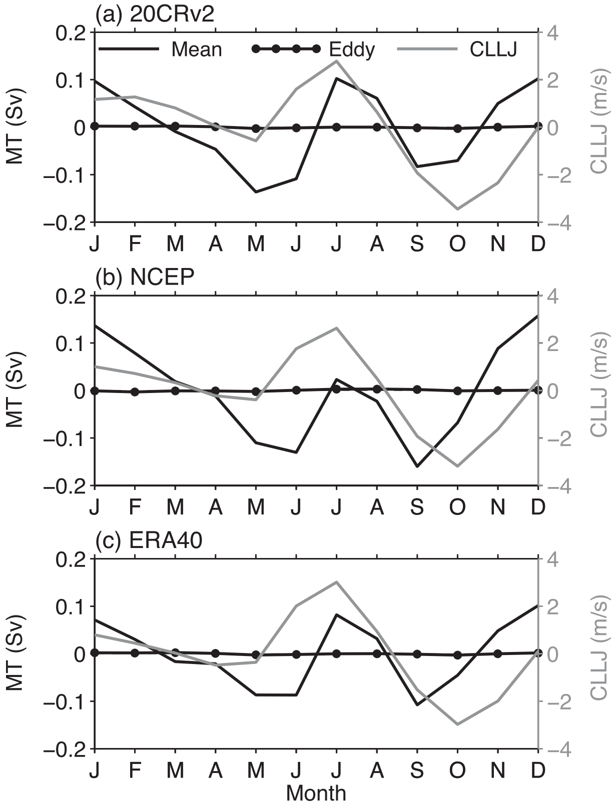


FIG. 3. Seasonal cycle of the moisture transport (MT) across Central America and the CLLJ (gray scale line, right ordinate) in (a) 20CRv2, (b) NCEP, and (c) ERA-40. The moisture transport contributed by monthly to longer time scales is denoted as the mean (black line) and the transient eddies (submonthly time scales) is represented as eddy (dotted line). The positive value represents a stronger CLLJ and a moisture transport from the Atlantic to the Pacific basin.

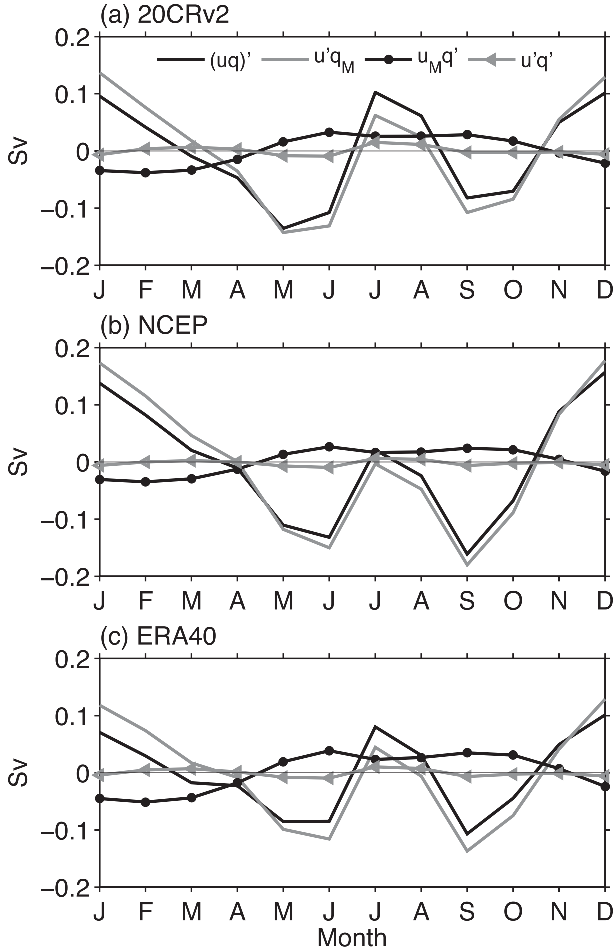


FIG. 4. Seasonal cycle of the moisture transport (monthly and longer time scale part) variations across Central America and the associated decomposed components in (a) 20CRv2, (b) NCEP, and (c) ERA-40.

### *c. Moisture transport across Central America*

Our analysis in the previous section has suggested the potential importance of moisture advection by the CLLJ in the seasonal variation of the EmP over the AWP. In this subsection, we address the CLLJ and its relationship with the moisture transport across Central America. Following previous studies (e.g., Wang 2007), we use the 925-hPa zonal wind in the region of 12.5°–17.5°N, 80°–70°W to measure the CLLJ. Figure 3 shows the seasonal variation of the CLLJ and the moisture transport from the Atlantic to the Pacific. All of the reanalysis datasets show a positive correlation between the CLLJ and the moisture transport contributed by the monthly mean part of $\mathrm{MT}_M$. The linear correlation coefficient is 0.63, 0.60, and 0.62 for the 20CRv2, NCEP, and ERA-40 reanalysis products, respectively. A strong (weak) CLLJ is associated with more (less) moisture export from the Atlantic to the Pacific. As expected, both the CLLJ and $\mathrm{MT}_M$ show a semiannual feature with two maxima in the winter and summer and two minima in the fall and spring. However, it can also be seen from Fig. 3 that the agreement between the two quantities in three reanalysis products is not perfect. The moisture transport contributed by the transient eddies is much smaller, which accounts for the total moisture transport by 6%, 4%, and 2% in 20CRv2, NCEP, and ERA-40, respectively.

Equation (12) shows that $\mathrm{MT}_M$ is dependent on the variation of $\overline{u}\,\overline{q}$. Here we further decompose the $\overline{u}\,\overline{q}$ change, $(\overline{u}\,\overline{q})'$, into the following components (overbar is omitted hereafter):

$$(uq)' = u'q_M + u_M q' + u'q', \tag{13}$$

where subscript $M$ denotes annual mean and the prime denotes the variation from the annual mean: that is, $q' = q - q_M$. This decomposition allows us to separate the effects of humidity and wind changes (Fig. 4). All of the three reanalysis products show that moisture transport from the Atlantic to the Pacific is primarily determined by the wind change, whereas the contribution by the humidity change is small. The nonlinear term of $u'q'$ is very small and can be ignored. A comparison of Figs. 3 and 4 shows that the CLLJ and $u'q_M$ are in phase, again suggesting that the CLLJ is important for the moisture transport across Central America. In spite of small amplitude, the humidity change can still make contribution to the moisture transport. The contribution by the humidity change ($u_M q'$) is an increase (decrease) of moisture transport during the summer and fall (winter and spring) as a result of the appearance (disappearance) of the AWP.

We have shown a link among the AWP, EmP in the AWP region, and the moisture transport across Central America. In association with the appearance (disappearance) of the AWP, less (more) moisture is exported from the Atlantic to the Pacific and more (less) precipitation occurs in the AWP region. This is because a large (small) AWP induces a low-level wind convergence (divergence), which favors (disfavors) local precipitation on one hand and also increases (decreases) the low-level westerly anomaly that decreases (increases) the moisture transport from the Atlantic to the Pacific on the other hand. However, there is an exception in July when precipitation is less (Fig. 2) and more moisture is transported across Central America (Figs. 3, 4) when the AWP is developed. This exception may result from the midsummer drought, the CLLJ variation, and the intrusion of the North Atlantic subtropical high. Finally, we note that the magnitudes of the moisture transport across Central America and EmP over the AWP are comparable on a seasonal time scale, implying that both of them can have a potential to affect ocean salinity (see next subsection) and then the Atlantic meridional overturning circulation (AMOC).

### *d. Seasonal cycle of sea surface salinity*

The AWP-modulated EmP and moisture transport across Central America can ultimately affect ocean salinity, especially sea surface salinity. Figure 5 shows the seasonal SSS cycle averaged over the AWP region. As expected, SSS is small (large) during the summer and fall (winter and spring) when the AWP appears (disappears) and the EmP and moisture transport across Central America are small (large). However, we have to keep in mind that the seasonal cycle of mixed layer salinity also depends on salinity advection, especially in the eastern part of the AWP where horizontal salinity advection is very important (Foltz and McPhaden 2008). All of the datasets of the direct observations and reanalysis products capture the seasonality of SSS in the AWP region, although the details is different. The SODA reanalysis product shares great similarity with the Argo observation, albeit with a smoother curve due to the relatively coarse resolution. This provides us a confidence to use SODA for analyzing the long-term variability of SSS in the following sections. SSS seasonality in GECCO and Ishii et al. seems to be overestimated, while the GFDL reanalysis tends to underestimate the SSS seasonal cycle over the AWP region.

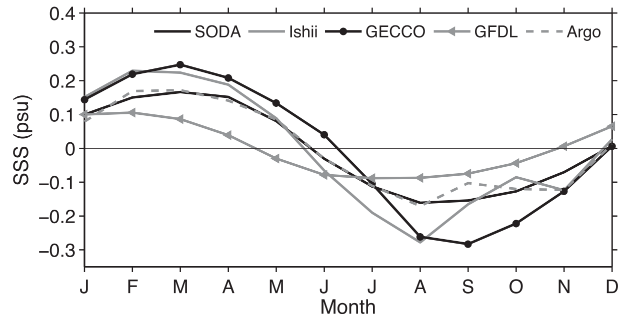


FIG. 5. Seasonal cycle of SSS over the AWP region based on various datasets of SODA, GECCO, GFDL, and Argo observations and *WOA05* data developed by Ishii et al. (2006).

## 4. Interannual variability

The freshwater flux in the AWP region also has significant interannual fluctuations. In this section, we examine and show the freshwater variability associated with the AWP, its associated mechanisms, moisture transport across Central America, and SSS on interannual time scales.

### *a. EmP variability*

We first compute the AWP index as the anomalies of the area of SST warmer than 28.5°C divided by the climatological AWP area (Wang et al. 2006, 2008a), as shown in Fig. 6a. The interannual AWP variability (Fig. 6b) is obtained by performing an 8-yr high-frequency filter to the detrended AWP index. We identify a warm pool 25% larger (smaller) than the climatological area as a large (small) warm pool; otherwise, the warm pool is classified as normal or neutral. Given that the AWP almost does not exist during winter and spring based on the definition of SST warmer than 28.5°C, we attempt to highlight the EmP anomalies associated with the AWP in summer (JJA) and fall [September–November (SON)]. The composites of the EmP anomalies for the large AWP (LAWP) and small AWP (SAWP) are shown in Fig. 7. All of the datasets show a similar pattern during JJA. The entire TNA experiences a reduced EmP when the AWP is large, with maximum values located in the

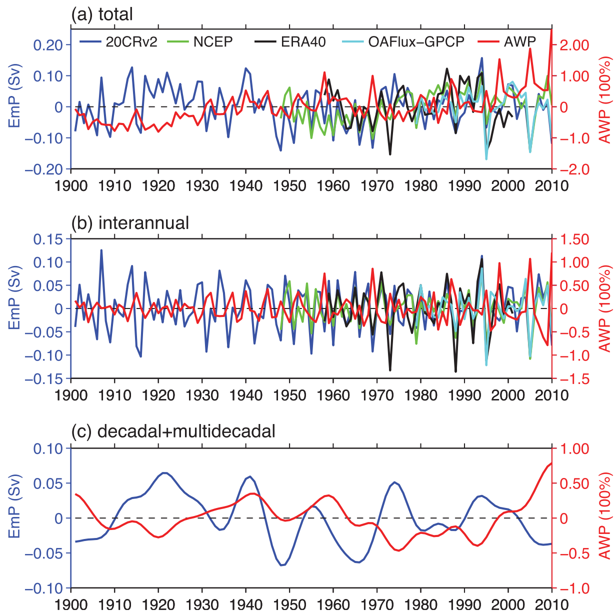


FIG. 6. Time series of the AWP area index (100%) and the integrated EmP anomalies (Sv) over the AWP region during the summer (JJA). The AWP area index is calculated by the extended reconstructed SST (ERSST) data, and the EmP anomalies are based on the datasets of 20CRv2, NCEP, ERA-40, and OAFlux–GPCP. Shown are the (a) total, (b) interannual, and (c) longer-term (decadal and multidecadal) variability. The interannual (longer term) variability is obtained by performing an 8-yr high (low) frequency filter to the detrended time series. In (c) only the 20CRv2 EmP time series is shown since other datasets are too short to examine longer-term variations.

AWP and the eastern ITCZ region, whereas there is an increased EmP in the west of subtropical North Atlantic and the tropical South Atlantic (Fig. 7, left). The opposite is true for SAWP (Fig. 7, right). The largest EmP anomalies in the AWP region can attain 0.8 mm day$^{-1}$. This indicates that the tropical North Atlantic Ocean is occupied by freshwater excess (deficit) when the AWP is large (small). During the fall, the EmP anomalies show similar response to that during the summer (not shown). Therefore, we only show and discuss plots during the summer in the following sections.

We also compute the time series of the EmP anomalies in the region of 5°–30°N from the American coast to 40°W and then compare it with the AWP index (Fig. 6). The first impression from Fig. 6 is that different datasets show different variations of the EmP anomalies. However, on interannual time scales all time series of the EmP anomalies show an out-of-phase relationship with the AWP index (Fig. 6b), with a large (small) AWP coinciding with a gain (loss) of freshwater to the ocean. This is consistent with the composite analysis in Fig. 7. The correlation coefficients are −0.40, −0.57, −0.36, and −0.50 in 20CRv2, NCEP, ERA-40, and OAFlux–GPCP, respectively, all of which are significant at the 95% confidence level.

### b. *Processes controlling the EmP anomalies*

As shown in Eqs. (2) and (5), the EmP anomalies are mainly determined by the changes contributed by the moisture divergence from the monthly mean [$\delta(\mathrm{div}Q_M)$] and the transient eddies [$\delta(\mathrm{div}Q_E)$]; $\delta(\mathrm{div}Q_M)$ can be further decomposed into the thermodynamics contribution ($\delta$TH) and the mean circulation dynamics contribution ($\delta$MCD). The composites of these terms for the large and small AWPs during JJA are shown in Fig. 8 based on the 20CRv2 dataset. Note that the ERA-40 and NCEP datasets are also analyzed, showing similar patterns to the 20CRv2 dataset. Since the 20CRv2 has much longer period than the ERA-40 and NCEP, we only present the results from the 20CRv2. A large portion of the EmP anomalies in the tropical Atlantic (Figs. 7a,b) can be accounted for by the moisture flux divergence variation of div$Q_M$ (Figs. 8a,b). The transient eddies of div$Q_E$ play a much smaller role than div$Q_M$ in the AWP region (Figs. 8c,d). However, the transient eddies do contribute to the EmP variability in the middle and high latitudes. This is an expected result since eddies are more active in high latitudes than low latitudes. A further calculation shows that the mean circulation dynamics contribution of $\delta$MCD is a major contributor to the variation of div$Q_M$ (Figs. 8e,f), while the role of $\delta$TH is very small (Figs. 8g,h).

The $\delta$MCD is contributed by the terms due to the wind divergence change ($\delta\mathrm{MCD}_D$) and the wind advection of humidity ($\delta\mathrm{MCD}_A$). Figures 9a–d show that $\delta\mathrm{MCD}_D$ is a dominant term, whereas $\delta\mathrm{MCD}_A$ is secondary. Given the dramatic decrease in specific humidity with height, the $\delta\mathrm{MCD}_D$ anomalies may come mainly from the low troposphere. In fact, the composites of the 925-hPa wind divergence anomalies for the large and small AWPs do confirm the result (Figs. 9e,f). During the large (small) AWPs, the low-level anomalous convergence (divergence) is associated with anomalous ascent (descent) in the middle troposphere (not shown) that decreases (increases) the EmP anomalies. The change of $\delta\mathrm{MCD}_A$ reflects primarily the change in low-level winds (Figs. 9g,h). Due to the small climatological humidity gradient in the AWP region, the wind changes do not induce a large contribution to the EmP anomalies. Figures 9g,h show that, in association with the large (small) AWPs, the CLLJ is significantly weakened (strengthened), implying that less (more) moisture is transported from the tropical Atlantic to the Pacific (which will be discussed and shown next).

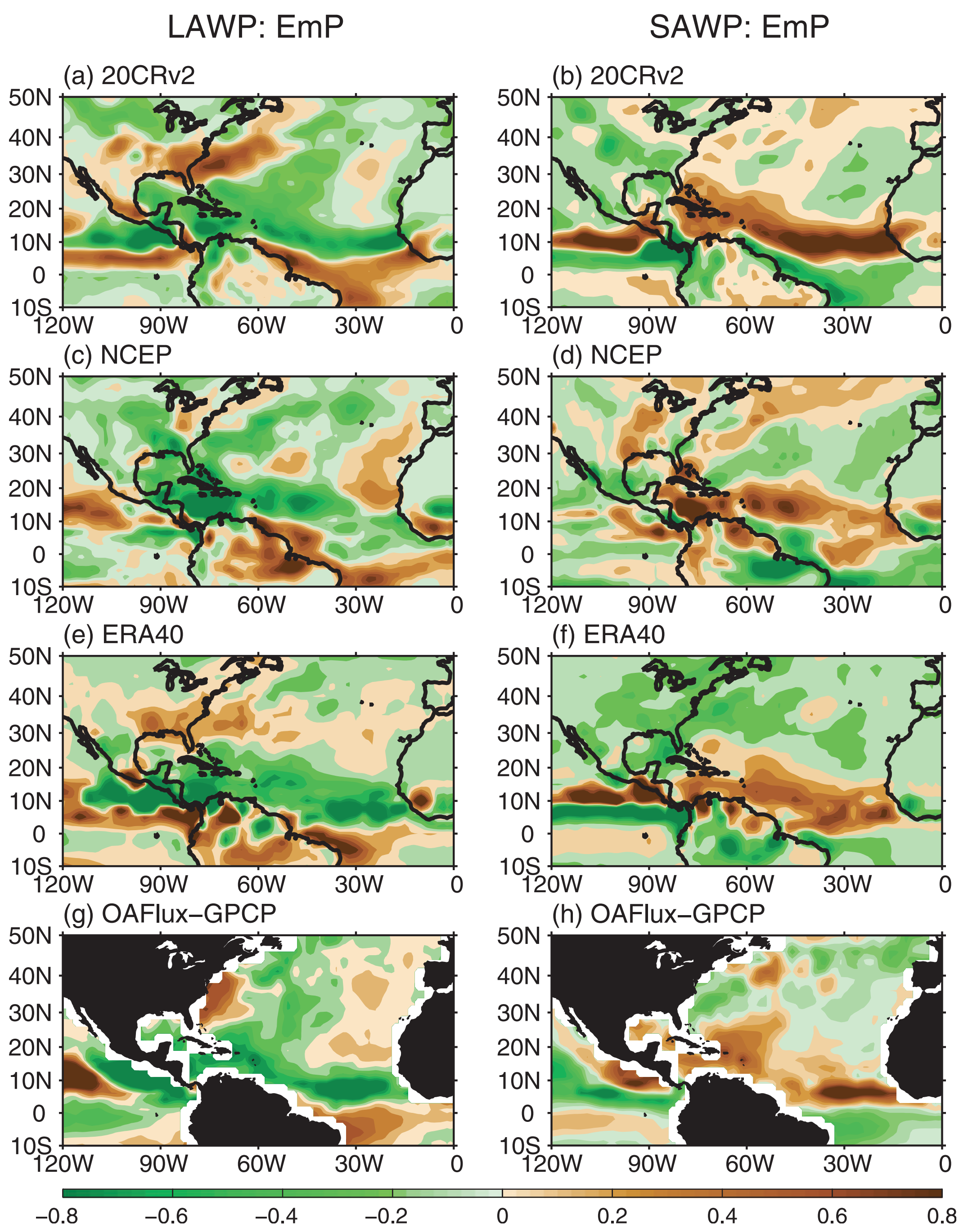


FIG. 7. Composites of the EmP anomalies (mm day$^{-1}$) on interannual time scales during the summer (JJA): (left) large AWP and (right) small AWP are shown for various datasets of (a),(b) 20CRv2; (c),(d) NCEP; (e),(f) ERA-40; and (g),(h) OAFlux–GPCP.

### c. *Moisture transport anomalies across Central America*

The composite analyses of the moisture transport anomalies across Central America for the large and small AWPs based on different datasets are shown in Fig. 10. All of the three reanalysis products show a consistent result, albeit with the difference in the transport magnitude. A large (small) AWP is associated with the negative (positive) moisture transport anomalies or less (more) moisture transport from the Atlantic to the Pacific. Like the seasonal cycle, this moisture transport

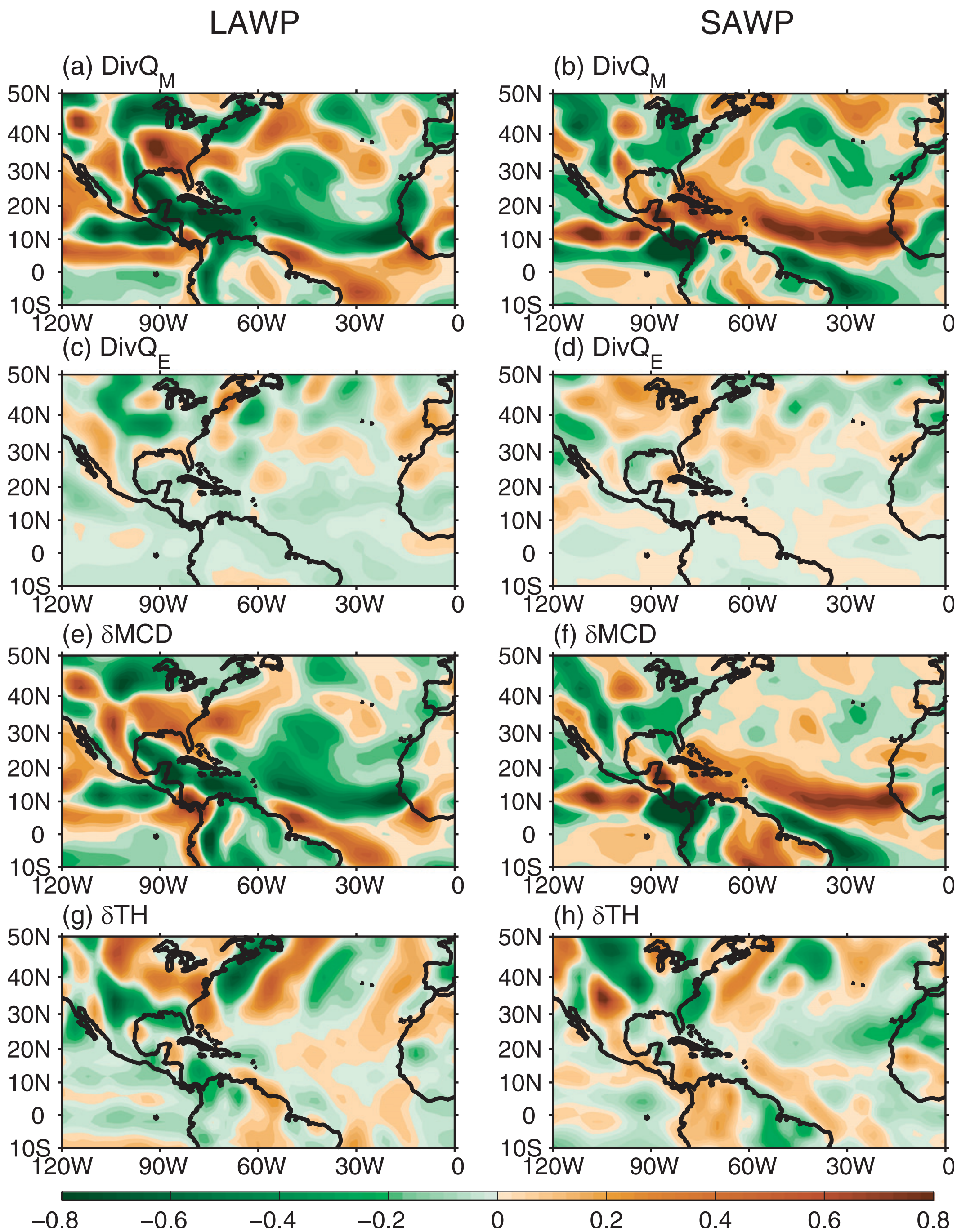


FIG. 8. Composites of the moisture flux divergence anomalies on interannual time scales for (left) large AWP and (right) small AWP during the summer (JJA): (a),(b) from monthly to longer time scales of div$Q_M$ and (c),(d) from the transient eddies of div$Q_E$. Here div$Q_M$ is further decomposed into (e),(f) the mean circulation dynamics contribution of $\delta$MCD and (g),(h) the thermodynamics contribution of $\delta$TH. Units are millimeters per day. The composites are calculated based on 20CRv2.

response is dominated by the wind change associated with the CLLJ variation (Fig. 9), whereas the specific humidity plays a minor and opposite contribution. This is easily understood. Because of the nonlinearity of the Clausius–Clapeyron equation, the specific humidity increases more over warm water than over cool water in the absence of any sizable change in relative humidity. Hence, moisture becomes increased (decreased) in response to

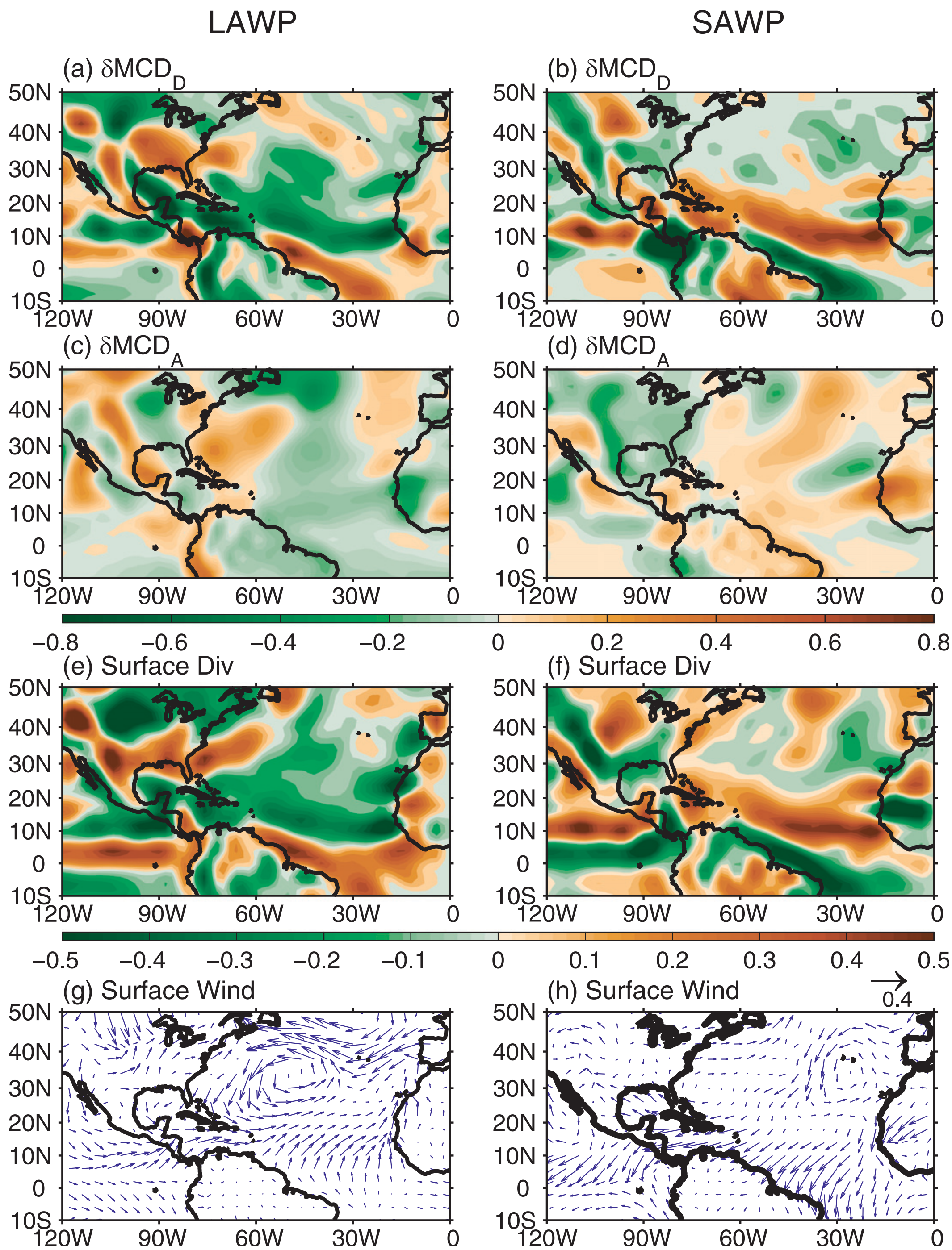


FIG. 9. Composites of the moisture change (mm day$^{-1}$), calculated based on 20CRv2, due to mean circulation dynamics on interannual time scales for (left) large AWP and (right) small AWP during the summer (JJA). The contribution by (a),(b) the wind divergent change and (c),(d) the advection of moisture by the wind change are shown. Composites of the 925-hPa (e),(f) wind divergence and (g),(h) wind anomalies are also shown.

a large (small) AWP, which in turn favors more (less) moisture transported to the Pacific. However, the specific humidity response cannot be overwhelmed by the role of wind change, which tends to reduce (increase) the easterly wind and thus generate a weakened (strengthened) moisture transport across Central America during a large (small) AWP. Note that the magnitude (peak-to-peak variation) of interannual moisture transport anomalies associated

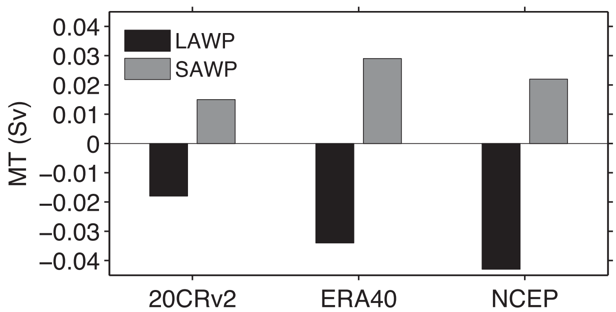


FIG. 10. Composites of the cross–Central America moisture transport anomalies on interannual time scales for large AWP and small AWP during the summer (JJA) using the datasets of 20CRv2, NCEP, and ERA-40.

with the AWP is about 0.06 Sv (Sv ≡ $10^6$ $m^3$ $s^{-1}$), which is much smaller than the long-term mean (0.26 Sv averaged in the three reanalysis products) and the seasonal cycle (0.4 Sv).

### *d. SSS anomalies*

As expected, SSS is characterized by the negative (positive) anomalies over the AWP region for a large (small) AWP in both the SODA reanalysis and Ishii et al. salinity data (Fig. 11). The SSS anomalies are consistent with the EmP response and moisture transport change across Central America (Fig. 7). This indicates that, to the first order, SSS variability over the AWP region associated with the AWP on the interannual time scales is balanced by the local freshwater flux. When the AWP is large (small), there is an anomalous low-level convergence (divergence) over the AWP region on one hand and a weakened (strengthened) trade wind across Central America on the other. The former tends to increase (decrease) precipitation and the latter tends to decrease (increase) the moisture transport across Central America, leading to more (less) water vapor in the AWP region. Both of these two effects favor generating negative (positive) SSS anomalies in the AWP region when the AWP is large (small).

## 5. Multidecadal variability

As shown in Fig. 6c, the EmP anomalies in the AWP region also vary on multidecadal time scales with the positive (negative) EmP anomalies coinciding with the small (large) AWP. Using the multidecadal AWP index, we identify the positive (negative) phase of the AWP as $AWP^+$ ($AWP^-$) by a warm pool 10% larger (smaller) than the climatological mean. Then we investigate the relationship of the EmP anomalies with the AWP on multidecadal time scales by making composites. As

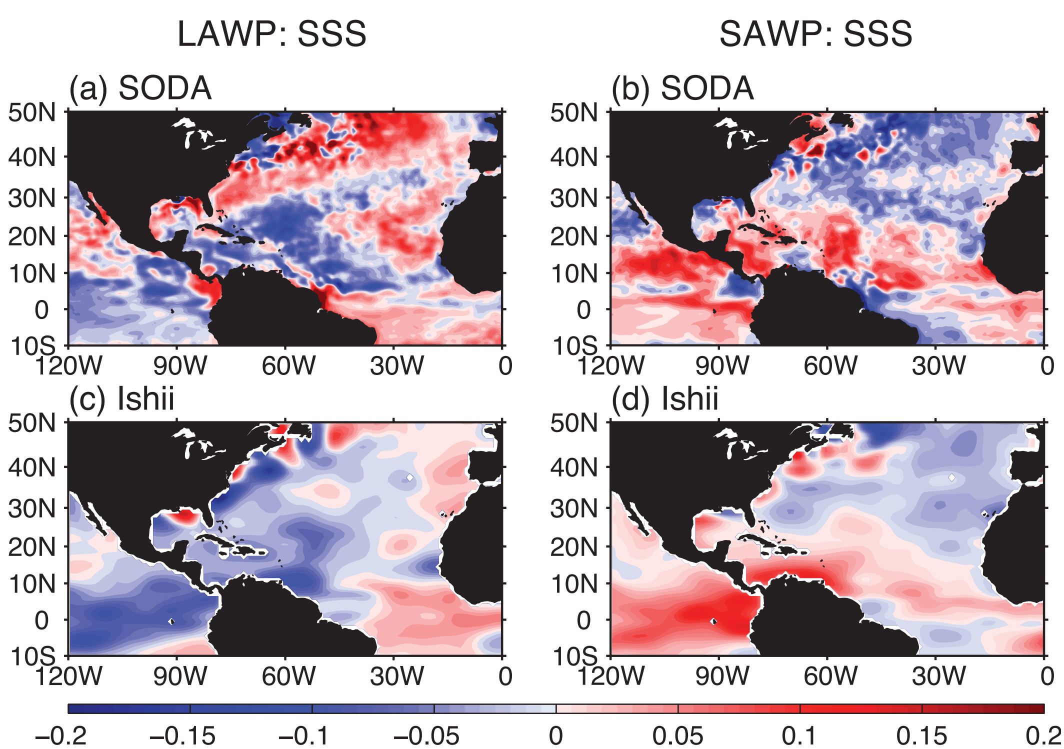


FIG. 11. Composites of the SSS anomalies (psu) on interannual time scales for large AWP and small AWP during summer (JJA) based on the SODA and Ishii et al. data.

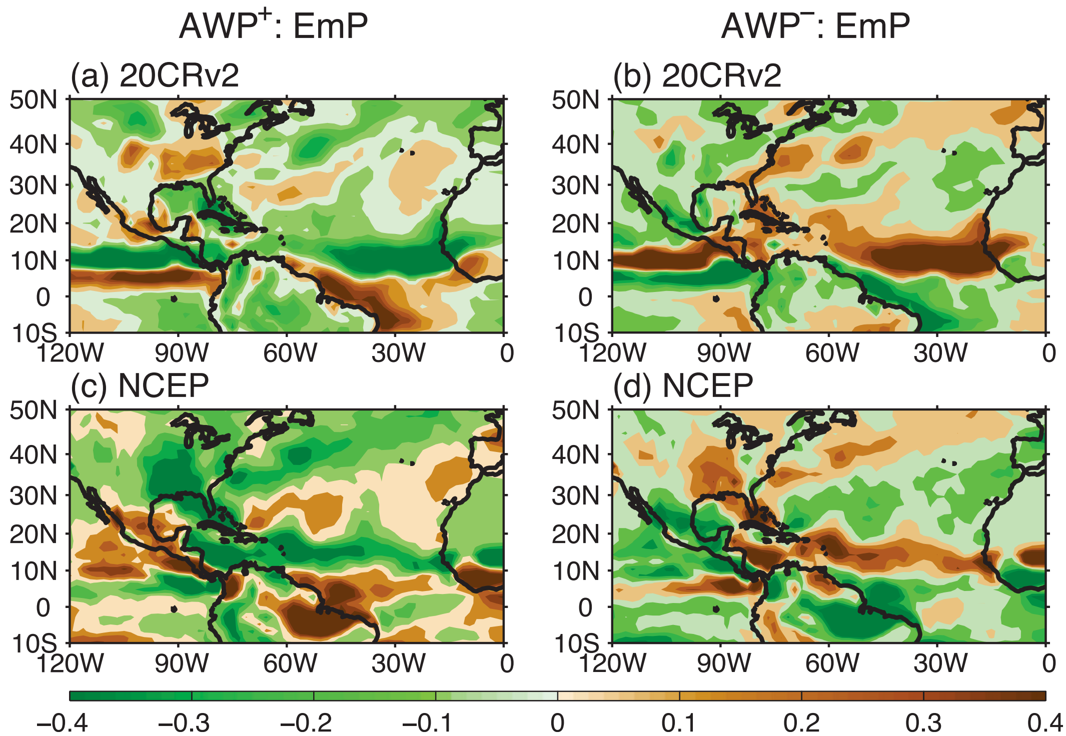


FIG. 12. Composites of the EmP anomalies (mm day$^{-1}$) on multidecadal time scales during summer (JJA) for (left) the positive phase of the AWP and (right) the negative phase of the AWP from the datasets of (a),(b) 20CRv2 and (c),(d) NCEP.

shown in Fig. 12, there is a net freshwater gain over the TNA during the warm phase of the AWP, particularly in the AWP and tropical eastern North Atlantic regions, and the opposite occurs during the cold phase of the AWP. Compared to the EmP variation on interannual time scales, the multidecadal variability of EmP exhibits a relatively smaller magnitude (Fig. 7 versus Fig. 12), which is also revealed in the time series (Figs. 6b,c) (but the multidecadal variability may be very important since it persists on a longer time scale). Similar to the interannual variability, the multidecadal change of EmP in the tropical Atlantic is balanced mainly by the moisture flux divergence of div$Q_M$ (Figs. 13a,b), whereas the contribution from the transient eddies of div$Q_E$ is very small (Figs. 13c,d). Again, the mean circulation dynamics of $\delta$MCD is a major contributor to div$Q_M$, whereas the thermodynamics contribution of $\delta$TH is very small (Figs. 13e–h). The contribution to the mean circulation dynamics primarily arises from $\delta\mathrm{MCD}_D$ (Figs. 14a,b), and $\delta\mathrm{MCD}_A$ is small and even opposite (Figs. 14c,d).

The effect of $\delta\mathrm{MCD}_D$ is also seen from the low-level anomalous wind divergence field (Figs. 14e,f). The tropical Atlantic is characterized by a dipole divergence field anomaly with an anomalous convergence in the north and an anomalous divergence in the south during the warm phase of the AWP, and vice versa during the cold phase of the AWP. This implies that the ITCZ has shifted toward the north (south) during the warm (cold) phase of the AWP. In association with the ITCZ shift, the Hadley circulation cell also shows a change. Figure 15 shows the climatological Hadley cell together with the change from the cold to warm phases to the AWP. It is clearly seen that the climatological Hadley cell ascends to the upper level around 10°N, diverges to the north and south when it reaches to the upper layer, and ultimately descends to the lower level at about 30°N. The difference between the AWP warm and cold phases shows the negative streamfunction anomalies over the climatological ascent region, indicating a northward (southward) shift of the Hadley cell.

Similar to the interannual variability, $\delta\mathrm{MCD}_A$ mainly reflects the changes in the low-level wind. As exhibited in Figs. 14g,h, the poleward flow corresponds to the negative EmP anomalies and the equatorward flow is associated with the positive EmP anomalies. A large (small) AWP on multidecadal time scales also coincides with a weakened (strengthened) CLLJ.

As expected, both the moisture transport and SSS on multidecadal time scales show a similar response to the interannual variation (Figs. 16 and 17). The moisture transport from the tropical Atlantic to the Pacific is also characterized by a reduced (increased) transport across

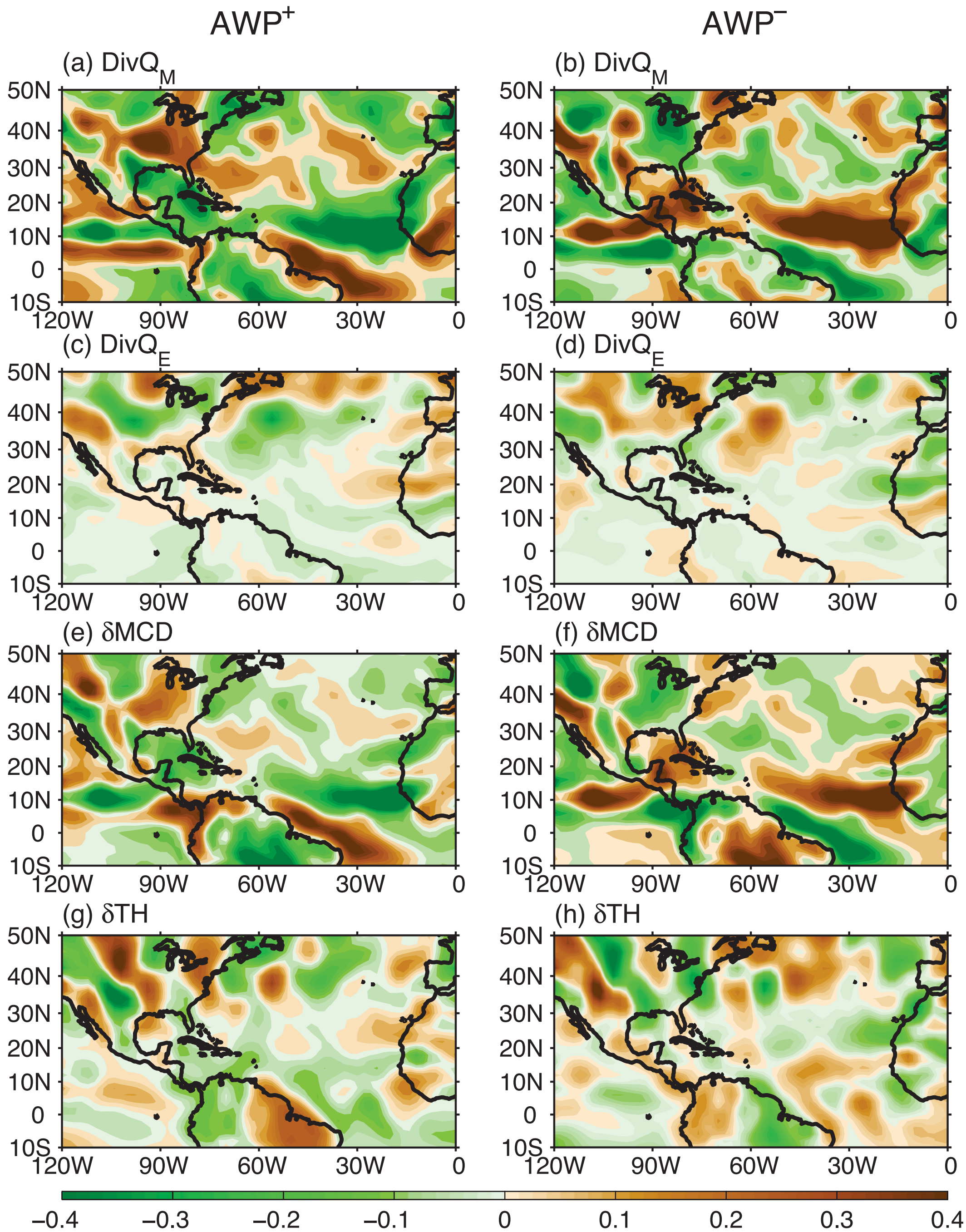


FIG. 13. Composites of the moisture flux divergence anomalies on multidecadal time scales during the summer (JJA) for (left) the positive phase of the AWP and (right) the negative phase of the AWP (a),(b) from monthly to longer time scales of div$Q_M$ and (c),(d) from the transient eddies of div$Q_E$. Here div$Q_M$ is further decomposed into (e),(f) the mean circulation dynamics contribution of δMCD and (g),(h) the thermodynamics contribution of δTH. Units are millimeters per day. The composites are calculated based on 20CRv2.

Central America during the warm (cold) phase of the AWP (Fig. 16). However, the amplitude of the multidecadal moisture transport is smaller than the interannual variation because of a small response of the CLLJ. Consistent with the distribution of the EmP anomalies and the moisture transport across Central America, the multidecadal SSS variability shows the negative (positive) anomalies in the AWP region.

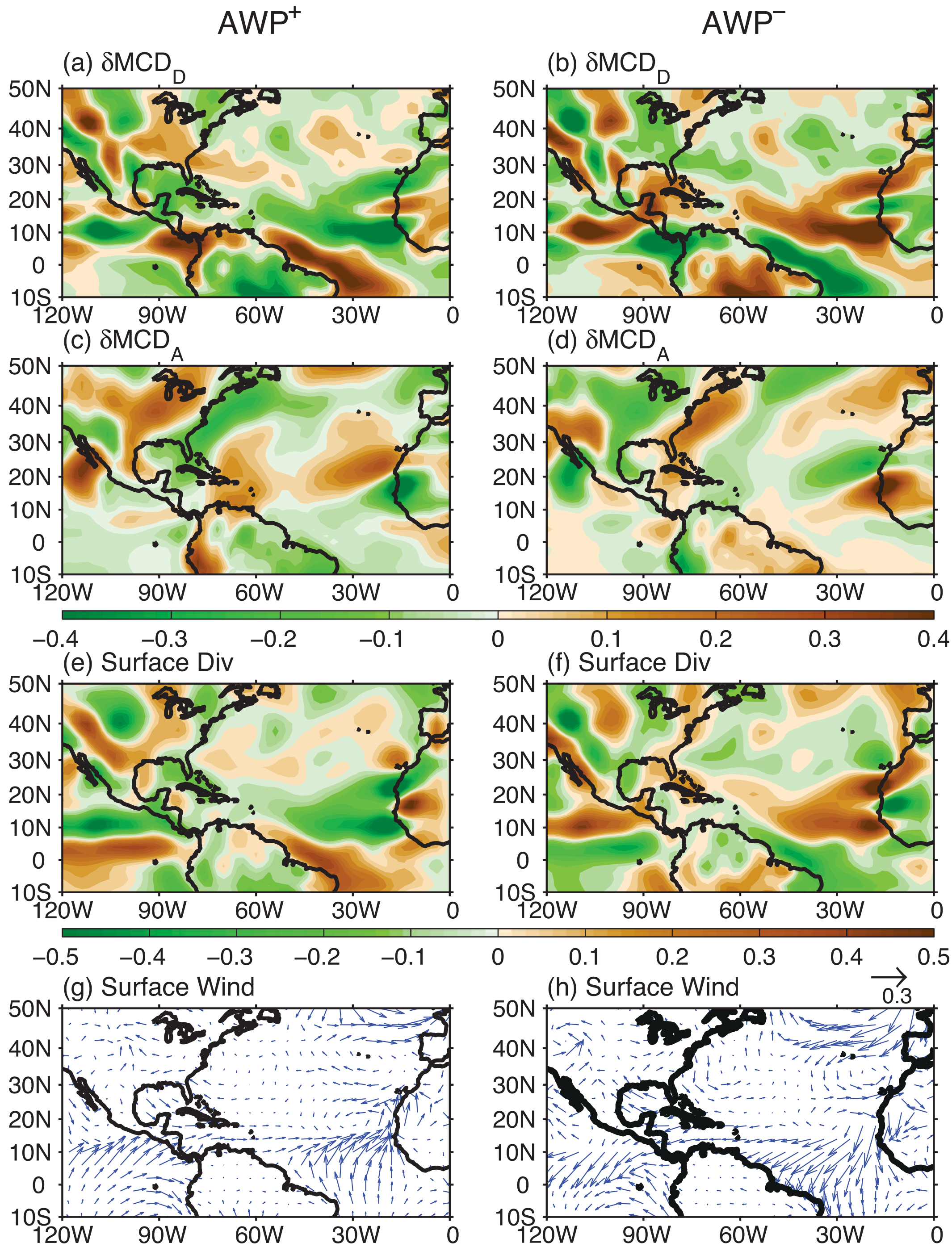


FIG. 14. Composites of the moisture change (mm day$^{-1}$), calculated based on 20CRv2, due to the mean circulation dynamics on multidecadal time scales during the summer (JJA) for (left) the positive phase of the AWP and (right) the negative phase of the AWP: the contribution by (a),(b) the wind divergent change and (c),(d) the advection of moisture by the wind change. Composites of the 925-hPa (e),(f) wind divergence and (g),(h) wind anomalies are also shown.

## 6. Summary and discussion

Various reanalysis products and observations are used in this paper to examine the response of freshwater flux and SSS to the AWP variability. All of the datasets show consistent and similar results for the variations of seasonal, interannual, and multidecadal time scales. A large (small) AWP is associated with an increased (decreased)

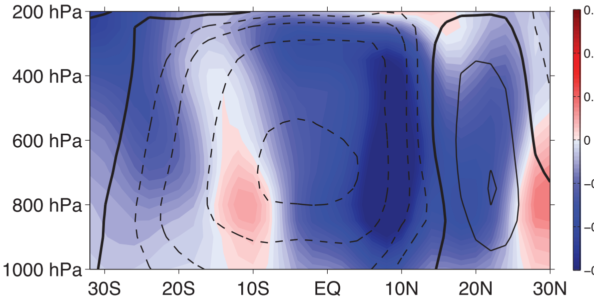


FIG. 15. The Hadley circulation during the summer (JJA), defined as the zonal-mean streamfunction in 20CRv2. Contours represent the climatological Hadley cell, and the shading denotes the difference of the Hadley cell between the positive and negative phases of the AWP on multidecadal time scales: contour interval $20 \times 10^9$ kg s$^{-1}$.

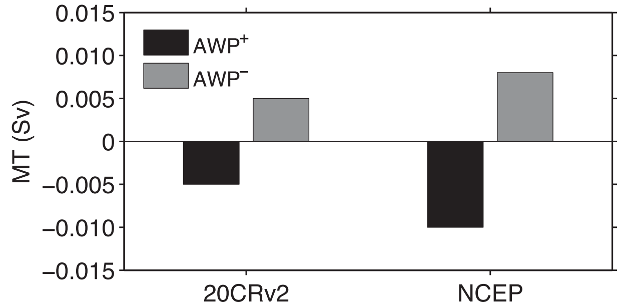


FIG. 16. Composites of the cross–Central America moisture transport anomalies (Sv) on multidecadal time scales during the summer (JJA) for the positive and negative phases of the AWP using the datasets of 20CRv2 and NCEP.

freshwater gain (loss) to the ocean, which is primarily due to the negative (positive) EmP anomalies and the decreased (increased) moisture transport from the Atlantic to Pacific basins across Central America. The moisture budget analyses show that the EmP anomalies are mainly balanced by the moisture flux divergence change primarily from the monthly to longer time scales, whereas the contribution from the transient eddies is much smaller. The moisture flux divergence change arises mainly from the change of the mean circulation dynamics (change in wind but no change in humidity), while the thermodynamics contribution (change in humidity but no change in wind) is of secondary importance. A further decomposition of the mean circulation dynamics demonstrates that the wind divergent change plays a dominant role and the advection of moisture by the wind change is small. Consistent with a previous modeling study (Wang et al. 2008b), the wind divergent change results from the warm SST anomalies in the AWP region. When the AWP is large (small), warm

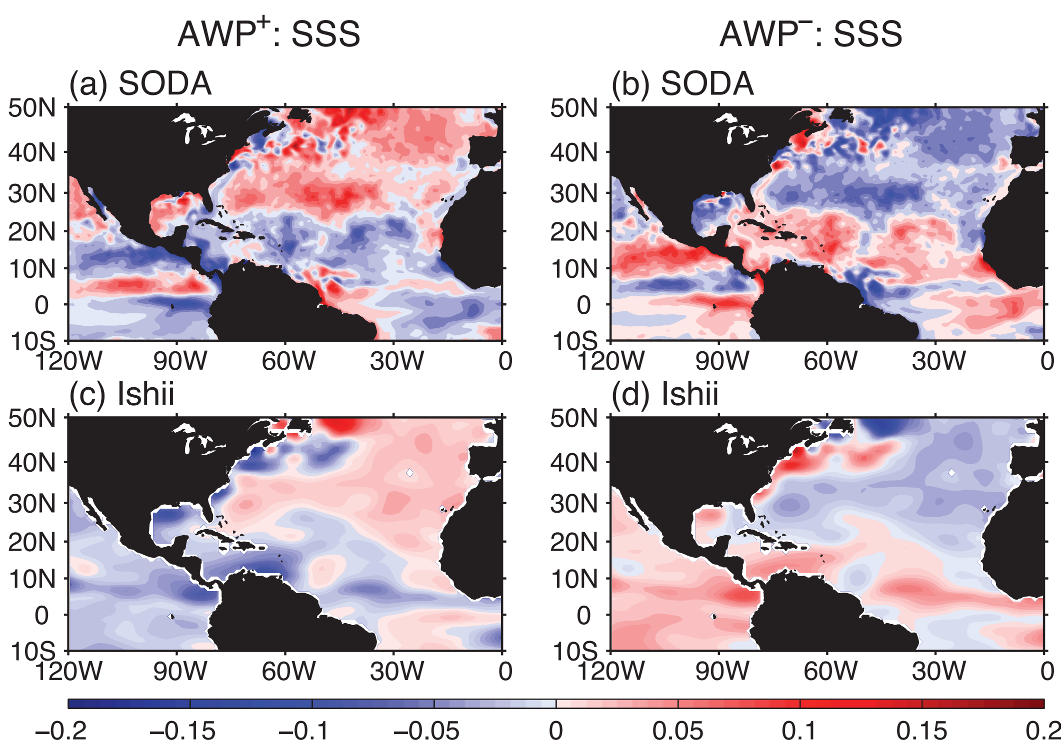


FIG. 17. Composites of the SSS anomalies (psu) on multidecadal time scales during the summer (JJA) for the (left) positive phase and (right) negative phase of the AWP based on the SODA and Ishii et al. data.

(cold) SST over the AWP region induces an anomalous convergence (divergence) in the low level according to the Gill (1980) theory, which induces an anomalous ascent (descent) motion and thus generates an increased (decreased) precipitation. Meanwhile, the divergent circulation change is associated with the north–south shift of the ITCZ, leading to an anomalous precipitation band over the tropical Atlantic.

On the other hand, a large (small) AWP is also associated with a weakening (strengthening) of the CLLJ and the westerly (easterly) anomalies across Central America. The wind change reduces (enhances) the moisture transport from the Atlantic to the Pacific, which in turn leads to more (less) moisture residing in the AWP region and, thus, generating more (less) local precipitation. Both local EmP and moisture transport changes can affect the ocean salinity ultimately. As expected, SSS variability associated with the AWP is characterized by the negative (positive) SSS anomaly response to a large (small) AWP.

Although the features and processes of the freshwater variations in the AWP are similar on seasonal, interannual, and multidecadal time scales, their magnitudes are quite different. The range or amplitude (peak-to-peak variation) of the AWP-modulated seasonality of the EmP anomalies has the largest value, reaching 0.6 Sv. The magnitude of interannual variability of EmP associated with the AWP in the summer is ~0.2 Sv, while the multidecadal variability has a smaller amplitude that can reach 0.15 Sv. Similarly, the moisture transport across Central America associated with the AWP has the largest magnitude in the seasonal cycle, which can reach 0.4 Sv. However, the cross–Central American moisture transport exhibits a smaller amplitude change in the summer on the interannual and multidecadal time scales, with amplitude about 0.06 Sv and 0.02 Sv, respectively. As a result, SSS has the largest amplitude in the seasonal cycle (0.6 psu); however, it only has 0.4 and 0.2 psu fluctuations on interannual and multidecadal time scales, respectively.

The results suggest a potential interaction between the AWP and the Atlantic meridional overturning circulation (AMOC) through the freshwater and salinity response. On one hand, as the AMOC weakens, its northward heat transport is reduced; thus, the North Atlantic cools and the AWP becomes small. On the other hand, a small AWP decreases rainfall in the TNA and increases the cross–Central American moisture export to the eastern North Pacific. Both of these factors tend to increase salinity in the tropical North Atlantic Ocean. Advected northward by the wind-driven ocean circulation (Thorpe et al. 2001; Vellinga and Wu 2004; Yin et al. 2006; Krebs and Timmermann 2007), the positive salinity anomalies may increase the upper-ocean density in the deep-water formation regions and thus strengthen the AMOC. Therefore, the AWP seems to play a negative feedback role that acts to restore the AMOC after it is weakened or shut down. This hypothesis needs to be tested and confirmed by using numerical model experiments. In particular, model experiments should address whether the AWP-related freshwater flux and the moisture export across Central America to the eastern Pacific are of significance for the strength of the AMOC, if the persistence of the anomaly is on a longer time scale (e.g., on the order of decades).

*Acknowledgments.* We thank Greg Foltz for serving as AOML's internal reviewer and two anonymous reviewers for their comments and suggestions. This work was supported by grants from National Oceanic and Atmospheric Administration/Climate Program Office, the base funding of NOAA/Atlantic Oceanographic and Meteorological Laboratory (AOML). The findings and conclusions in this report are those of the author(s) and do not necessarily represent the views of the funding agency.

## REFERENCES

Adler, R. F., and Coauthors, 2003: The version-2 Global Precipitation Climatology Project (GPCP) monthly precipitation analysis (1979–present). *J. Hydrometeor.,* **4,** 1147–1167.

Broecker, W. S., 1997: Thermohaline circulation, the Achilles heel of our climate system: Will man-made $CO_2$ upset the current balance? *Science,* **278,** 1582–1588.

Carton, J. A., and B. S. Giese, 2008: A reanalysis of ocean climate using Simple Ocean Data Assimilation (SODA). *Mon. Wea. Rev.,* **136,** 2999–3017.

Compo, G. P., and Coauthors, 2011: The Twentieth Century Reanalysis project. *Quart. J. Roy. Meteor. Soc.,* **137,** 1–28.

Foltz, G. R., and M. J. McPhaden, 2008: Seasonal mixed layer salinity balance of the tropical North Atlantic Ocean. *J. Geophys. Res.,* **113,** C02013, doi:10.1029/2007JC004178.

Gibson, J. K., P. Kållberg, S. Uppala, A. Nomura, A. Hernandez, and E. Serrano, 1997: ERA description. ECMWF Re-Analysis Project Rep. 1, 71 pp.

Gill, A. E., 1980: Some simple solutions for heat-induced tropical circulation. *Quart. J. Roy. Meteor. Soc.,* **106,** 447–462.

Ishii, M., M. Kimoto, K. Sakamoto, and S. I. Iwasaki, 2006: Steric sea level changes estimated from historical ocean subsurface temperature and salinity analyses. *J. Oceanogr.,* **62,** 155–170.

Kalnay, E., and Coauthors, 1996: The NCEP/NCAR 40-Year Reanalysis Project. *Bull. Amer. Meteor. Soc.,* **77,** 437–471.

Katsumata, K., and H. Yoshinari, 2010: Uncertainties in global mapping of Argo drift data at the parking level. *J. Oceanogr.,* **66,** 553–569.

Kõhl, A., D. Dommenget, K. Ueyoshi, and D. Stammer, 2006: The global ECCO 1952 to 2001 ocean synthesis. ECCO Tech. Rep. 40, 44 pp. [Available online at http://www.ecco-group.org/ecco1/report/report_40.pdf.]

Krebs, U., and A. Timmermann, 2007: Tropical air–sea interactions accelerate the recovery of the Atlantic meridional overturning circulation after a major shutdown. *J. Climate,* **20,** 4940–4956.

Magana, V., J. A. Amador, and S. Medina, 1999: The midsummer drought over Mexico and Central America. *J. Climate,* **12,** 1577–1588.

Mapes, B. E., P. Liu, and N. Buenning, 2005: Indian monsoon onset and the Americas midsummer drought: Out-of-equilibrium response to smooth seasonal forcing. *J. Climate,* **18,** 1109–1115.

Peixoto, J. P., and A. H. Oort, 1992: *Physics of Climate.* American Institute of Physics, 520 pp.

Richter, I., and S.-P. Xie, 2010: Moisture transport from the Atlantic to the Pacific basin and its response to North Atlantic cooling and global warming. *Climate Dyn.,* **35,** 551–566.

Romanova, V., M. Prange, and G. Lohmann, 2004: Stability of the glacial thermohaline circulation and its dependence on the background hydrological cycle. *Climate Dyn.,* **22,** 527–538.

Rosati, A., M. Harrison, A. Wittenberg, and S. Zhang, 2004: NOAA/GFDL ocean data assimilation activities. *Proc. CLIVAR Workshop on Ocean Reanalysis,* NCAR, Boulder, CO, 25–26.

Seager, R., N. Naik, and G. A. Vecchi, 2010: Thermodynamic and dynamic mechanisms for large-scale changes in the hydrological cycle in response to global warming. *J. Climate,* **23,** 4651–4668.

Thorpe, R. B., J. M. Gregory, T. C. Johns, R. A. Wood, and J. F. B. Mitchell, 2001: Mechanisms determining the Atlantic thermohaline circulation response to greenhouse gas forcing in a non-flux-adjusted coupled climate model. *J. Climate,* **14,** 3102–3116.

Trenberth, K. E., and C. J. Guillemot, 1995: Evaluation of the global atmospheric moisture budget as seen from analyses. *J. Climate,* **8,** 2255–2272.

Vellinga, M., and P. Wu, 2004: Low-latitude freshwater influences on centennial variability of the Atlantic thermohaline circulation. *J. Climate,* **17,** 4498–4511.

Wang, C., 2007: Variability of the Caribbean low-level jet and its relations to climate. *Climate Dyn.,* **29,** 411–422.

——, and D. B. Enfield, 2001: The tropical Western Hemisphere warm pool. *Geophys. Res. Lett.,* **28,** 1635–1638.

——, and ——, 2003: A further study of the tropical Western Hemisphere warm pool. *J. Climate,* **16,** 1476–1493.

——, and S.-K. Lee, 2007: Atlantic warm pool, Caribbean low-level jet, and their potential impact on Atlantic hurricanes. *Geophys. Res. Lett.,* **34,** L02703, doi:10.1029/2006GL028579.

——, D. B. Enfield, S.-K. Lee, and C. W. Landsea, 2006: Influences of the Atlantic warm pool on Western Hemisphere summer rainfall and Atlantic hurricanes. *J. Climate,* **19,** 3011–3028.

——, S.-K. Lee, and D. B. Enfield, 2007: Impact of the Atlantic warm pool on the summer climate of the Western Hemisphere. *J. Climate,* **20,** 5021–5040.

——, ——, and ——, 2008a: Atlantic warm pool acting as a link between Atlantic multidecadal oscillation and Atlantic tropical cyclone activity. *Geochem. Geophys. Geosyst.,* **9,** Q05V03, doi:10.1029/2007GC001809.

——, ——, and ——, 2008b: Climate response to anomalously large and small Atlantic warm pools during the summer. *J. Climate,* **21,** 2437–2450.

Xie, P., and P. A. Arkin, 1997: Global precipitation: A 17-year monthly analysis based on gauge observations, satellite estimates, and numerical model outputs. *Bull. Amer. Meteor. Soc.,* **78,** 2539–2558.

Yin, J., M. E. Schlesinger, N. G. Andronova, S. Malyshev, and B. Li, 2006: Is a shutdown of the thermohaline circulation irreversible? *J. Geophys. Res.,* **111,** D12104, doi:10.1029/2005JD006562.

Yu, L., and R. A. Weller, 2007: Objectively analyzed air–sea heat flux for the global ice-free oceans (1981–2005). *Bull. Amer. Meteor. Soc.,* **88,** 527–539.

Zaucker, F., and W. S. Broecker, 1992: The influence of atmospheric moisture transport on the fresh water balance of the Atlantic drainage basin: General circulation model simulations and observations. *J. Geophys. Res.,* **97,** 2765–2773.